

Quantifying cerebral blood arrival times using hypoxia-mediated arterial BOLD contrast

Alex A. Bhogal^{a,*}, Ece Su Sayin^b, Julien Poublanc^c, James Duffin^{b,d}, Joseph A. Fisher^{b,e}, Olivia Sobczyk^{c,e}, David J. Mikulis^c

^a Center of Imaging Sciences, High Field Department, University Medical Center Utrecht, Heidelberglaan 100, Utrecht, CX 3584, the Netherlands

^b Department of Physiology, University of Toronto, Toronto, Canada

^c Joint Department of Medical Imaging and the Functional Neuroimaging Lab, University Health Network, Toronto, ON, Canada

^d Toronto General Hospital Research Institute, Toronto, Canada

^e Department of Anesthesiology and Pain Medicine, University Health Network and University of Toronto, Toronto, Canada

ARTICLE INFO

Keywords:

Hypoxia
Blood arrival time
SAO₂ hemodynamics
Vascular
MRI
BOLD
CVR

ABSTRACT

Cerebral blood arrival and tissue transit times are sensitive measures of the efficiency of tissue perfusion and can provide clinically meaningful information on collateral blood flow status. We exploit the arterial blood oxygen level dependent (BOLD) signal contrast established by precisely decreasing, and then increasing, arterial hemoglobin saturation using respiratory re-oxygenation challenges to quantify arterial blood arrival times throughout the brain. We term this approach the Step Hemoglobin re-Oxygenation Contrast Stimulus (SHOCS). Carpet plot analysis yielded measures of signal onset (blood arrival), global transit time (gTT) and calculations of relative total blood volume. Onset times averaged across 12 healthy subjects were 1.1 ± 0.4 and 1.9 ± 0.6 for cortical gray and deep white matter, respectively. The average whole brain gTT was 4.5 ± 0.9 s. The SHOCS response was 1.7 fold higher in grey versus white matter; in line with known differences in tissue-specific blood volume fraction. SHOCS was also applied in a patient with unilateral carotid artery occlusion revealing ipsilateral prolonged signal onset with normal perfusion in the unaffected hemisphere. We anticipate that SHOCS will further inform on the extent of collateral blood flow in patients with upstream steno-occlusive vascular disease, including those already known to manifest reductions in vasodilatory reserve capacity or vascular steal.

1. Introduction

Cerebral blood arrival time (BAT) and regional or global transit times (rTT or gTT) show variation in the healthy human brain. These parameters are sensitive measures of the efficiency of tissue perfusion, potentially providing the ability to assess the status and effectiveness of upstream blood availability versus downstream small vessel flow control. Vascular diseases alter BAT and gTT, and mapping alterations of these metrics could prove useful in assessing the impact of vascular disease on the cerebral circulation in a clinically meaningful manner. More specifically, arterial hemodynamic measures would identify the presence and effectiveness of collateral blood supply (van Osch et al., 2018). For instance, collateralization of leptomeningeal vessels is a predictor of favorable outcome after stroke due to the ability to maintain perfusion in the ischemic penumbra for longer periods of time (McVerry et al., 2012). Similarly, an intact circle-of-Willis and/or strong leptomeningeal collaterals have been shown to protect against perfusion deficit in cases of significant carotid artery stenosis (Hartkamp et al., 2011;

Sebök et al., 2021). Establishing the extent of arterial collateralization and auto-regulatory capacity can provide a means to guide treatment decisions (Sebök et al., 2022) and potentially predict outcomes.

There are several Magnetic Resonance Imaging (MRI) based techniques available that can provide insights into arterial hemodynamics including arterial spin labeling (ASL), and dynamic susceptibility contrast (DSC) MRI. ASL is appealing in that it can provide quantification of cerebral blood flow (CBF). When combined with vasoactive stimuli such as hypercapnic challenges or the injection of acetazolamide, pre- and post-stimulus data can be combined to reveal cerebrovascular reactivity (CVR). When acquired with a multi post labeling delay (multi-PLD) scheme (Okell et al., 2019), ASL can hint at collateralization via the presence of arterial transit artifacts (Zaharchuk, 2020) (ATA), prolonged arterial transit times (ATT (Lou et al., 2017) or bolus arrival time (BAT (Paling et al., 2014))). However, ASL is a generally low signal-to-noise (SNR) modality with limited sensitivity in white matter (WM), and the temporal hemodynamic parameters rely on modeling the ASL kinetics (Buxton et al., 1998). DSC is also able to provide temporal information

* Corresponding author.

E-mail address: a.bhogal@umcutrecht.nl (A.A. Bhogal).

<https://doi.org/10.1016/j.neuroimage.2022.119523>.

Received 20 April 2022; Received in revised form 20 July 2022; Accepted 25 July 2022

Available online 27 July 2022.

1053-8119/© 2022 The Author(s). Published by Elsevier Inc. This is an open access article under the CC BY license (<http://creativecommons.org/licenses/by/4.0/>)

by tracking the passage of an injected contrast bolus using rapidly acquired gradient echo images. Using tracer kinetic modeling, perfusion measures as well as mean transit time (MTT) and time to peak (TTP) can be derived, which may also reflect collateralization (Seiler et al., 2021) or impaired hemodynamics. Nonetheless, DSC-MRI is invasive and relies on kinetic modelling to determine the arterial input function, errors in which are propagated to the calculation of hemodynamic parameters.

CVR mapping based on Blood oxygen level dependent (BOLD-CVR) in combination with hypercapnic stimuli, has been proposed as a marker for the availability of collateral blood flow (Sobczyk et al., 2020). BOLD-CVR measures reflect local changes in blood flow reflecting the net of widespread local changes in vascular resistance (Duffin et al., 2017). Such data however does not directly reflect the adequacy of local perfusion compensation. In addition, stimulated vasodilation can lead to local changes in blood velocity, affecting blood arrival times (Donahue et al., 2014). Most importantly, vascular steal and/or redistribution of blood flow may further disrupt the resting blood arrival and transit times in both healthy and diseased vascular beds. In contrast to BOLD response to hypercapnia and in common with DSC, deoxy-hemoglobin can be recruited as an arterial contrast agent (Poubanc et al., 2021; Vu et al., 2021). By manipulating blood oxygen saturation at the lungs, commensurate changes of deoxy-hemoglobin concentration in arterial blood can act as a contrast SHOCS to evoke signal changes reflecting hemodynamics at rest.

To test this concept, 12 healthy subjects were scanned using a continuous BOLD acquisition throughout a transient hypoxia breathing paradigm. We term this approach the Step Hemoglobin re-Oxygenation Contrast Stimulus (SHOCS). A combination of hemodynamic lag mapping and a modified carpet plot analysis (Fitzgerald et al., 2021) were applied to generate whole-brain onset maps representing the arrival of the deoxy-hemoglobin relative to the first responding voxels. In a single subject, a comparison is made between hypercapnic (BOLD-CVR) and SHOCS revealing a striking differences in hemodynamic response characteristics. Finally, SHOCS is tested in a patient with unilateral carotid artery occlusion to reveal extended onset times consistent with presumed limitations in collateral blood flow via the circle-of-Willis and/or leptomeningeal vessel network. We propose that quantifying the onset of immediate signal changes induced by the arrival of a deoxy-hemoglobin bolus in brain tissues, provides a measure of arterial blood arrival time. Delays in this onset time relative to other regions or a healthy cohort may reflect longer or slower transit paths through the cerebral vasculature.

2. Methods

2.1. Data acquisition

Data was selected from ongoing studies that are approved by the Research Ethics Board of the University Health Network and conform to the Declaration of Helsinki. Written informed consent was obtained from all subjects. MRI datasets from twelve healthy control subjects (33 ± 14 years old, 4 female) were analyzed. An additional patient with a unilateral carotid artery occlusion (CAO) was also included.

The study was performed using a 3-Tesla scanner (HDx Signa platform, GE healthcare, Milwaukee, WI, USA) with an 8-channel head coil. T2*-weighted gradient echo-planar imaging sequence with the following parameters: TE/TR = 30/1500 ms, flip angle = 73° , 29 slices, voxel size = 3 mm isotropic voxels, matrix size = 64×64 , simultaneous multi-slice factor (SMS) = 2. In the two cases in which a hypercapnic stimulus was applied (outlined below) a slightly modified BOLD acquisition was performed for increased spatial coverage: TR = 2400 ms, slices = 42, voxel size = 3.5 mm isotropic). A high-resolution T1-weighted spoiled-gradient-echo sequence was acquired for registration and tissue segmentation purposes with the following parameters: TI = 450 ms, TR 7.88 ms, TE = 3ms, flip angle = 12° , voxel size = $0.859 \times 0.859 \times 1$ mm, matrix

size = 256×256 , 146 slices, field of view = 24×24 cm, no inter-slice gap

A gas blender with a sequential gas delivery breathing circuit (RespirAct, Thornhill Research, Canada) was used to deliver two sequential hypoxic boluses while maintaining iso-capnea during BOLD acquisition. The hypoxic breathing protocol consisted of a 60 second baseline period in which end-tidal O_2 ($P_{ET}O_2$) was targeted at 95 mmHg, followed by a 60 second step down to 40 mmHg, then a return to baseline for 20s targeting 95 mmHg, then a second step down again targeting 40 mmHg, and then a final return to baseline at 95 mmHg $P_{ET}O_2$. A measured $P_{ET}O_2$ trace is shown in Fig. 1B. In a single control subject, an additional CO_2 challenge was applied consisting of clamping end-tidal partial pressure of CO_2 ($P_{ET}CO_2$) at the subjects resting level for 2 min, followed by an isoxic step increase of 10 mmHg for 2 min and return to baseline for another 2 min. $P_{ET}CO_2$ was then reduced by 10mmHg below baseline for 1 min, followed by a steady rise in $P_{ET}CO_2$ to 15mmHg above baseline over ~5 min, and returned to baseline for 2 min (see Fig. 4B: bottom).

2.2. Removal of large vessel contributions

A threshold step was applied to generate a modified whole-brain anatomical mask aimed at removing signal contributions from large veins that might contaminate arterial responses or strongly influence subsequent analysis steps. First, the inverse temporal signal to noise ratio (tNSR) was calculated for each voxel in the source BOLD data. Then voxels with tNSR values greater than the 98th percentile were identified and voxels were removed from the input brain mask (see Fig. S1).

2.3. Lag mapping

Voxel-wise SHOCS data were linearly de-trended and temporally de-noised using a wavelet based approach (Champagne and Bhogal, 2021). Time-series were decomposed using the 'sym4' mother wavelet and signals were then de-noised by applying a hard Bayesian threshold to the resulting wavelet coefficients. Data were then spatially smoothed using a 3D Gaussian kernel (filter width: 5 voxels, FWHM: 5 mm). Processed SHOCS data and end-tidal O_2 ($P_{ET}O_2$) data were interpolated by a factor 5 (effective TR: 300ms) to identify sub-TR signal displacements. Data were subsequently used to generate hemodynamic lag maps using a modified Rapidtide (Donahue et al., 2016; Frederick et al., 2012) approach implemented in the Matlab-based seeVR toolbox (Bhogal, 2021). In brief, a manual alignment between the end-tidal O_2 ($P_{ET}O_2$) and average grey matter (GM) signal was performed to minimize alignment errors that may occur to noise and motion-related signal spikes when using automated methods. Next, $P_{ET}O_2$ traces were correlated with GM voxels (excluding large vessels) and voxels having a Pearson correlation higher than 0.7 were isolated and temporally aligned for principal component analysis. Principal components explaining at least 85% of the signal variability were extracted to generate a new regressor. The new regressor was then correlated against all GM voxels and this process was repeated until the root mean square error between subsequent regressor was less than 0.005. This convergence process resulted in an optimized SHOCS regressor. Hemodynamic lags were calculated using a shifted general linear model (GLM) approach that minimized the co-efficient of determination (R-squared) to select the shifted regressor that explained most of the SHOCS signal variance. Finally, a linear regression between the $P_{ET}O_2$ trace and each voxels' signal trace was performed. The slope of this regression provided the hypoxic signal response.

2.4. Carpet plot analysis

Lag values were used to sort individual voxel time-series, which were then listed to produce 2-D carpet plots (Fig. 1C). The original work by Fitzgerald et al. (2021) applied the carpet plot analysis to derive the presumed transit times of blood borne signals observed in resting-state

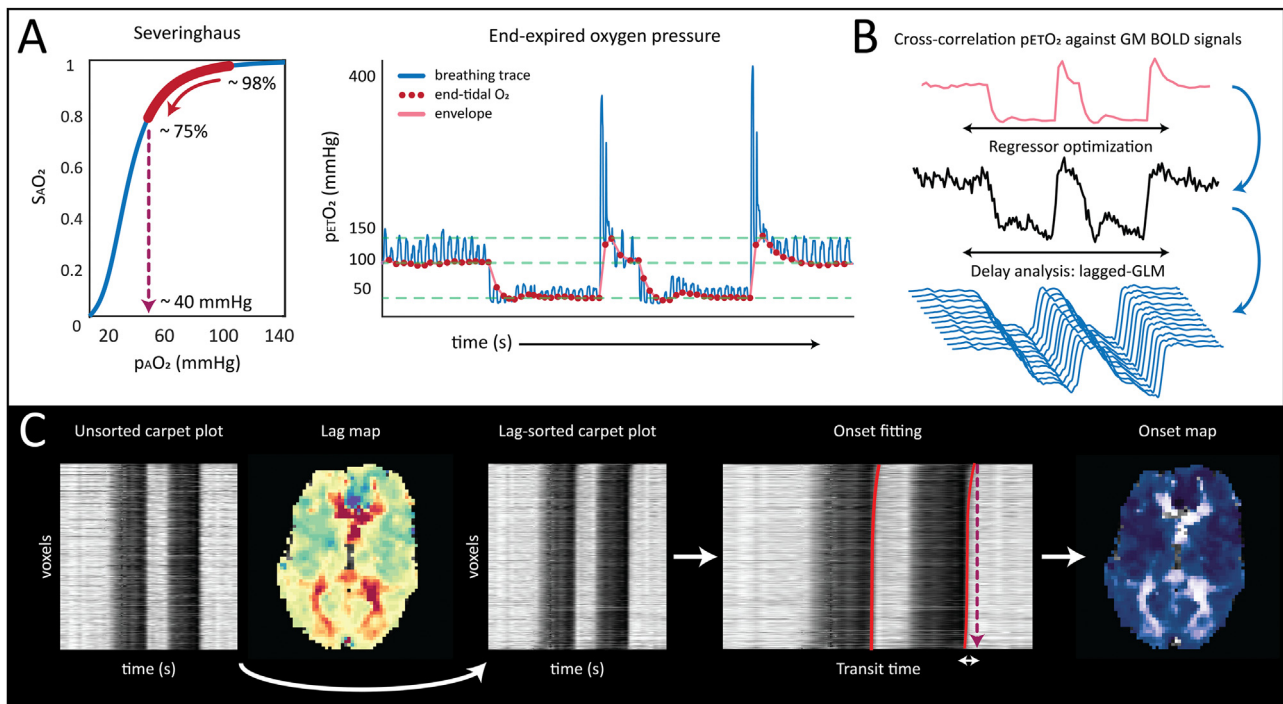


Fig. 1. Process diagram for generating onset maps based on the hypoxic SHOCS breathing paradigm (A): arterial oxygen tension is manipulated using a RespirAct system. Arterial oxygen pressure is targeted at 45 mmHg which, according to the Severinghaus equation (Severinghaus, 1979), leads to a predicted arterial hemoglobin saturation of approximately 75%; (B): resulting BOLD data, along with the end-tidal O_2 trace are provided as input for the hemodynamic lag calculation algorithm. This process involves the generation of an optimized BOLD signal probe which is regressed against each voxel time-series at progressive lag increments; (C): the resulting hemodynamic lag values are then used to sort BOLD voxels in order on increasing lag. By plotting voxels as a list, a carpet plot is produced. Signal transitions driven by the BOLD signal onset are fit using a non-linear spline function and the resulting onset times are re-mapped into the native BOLD space to produce onset maps.

fMRI under the assumption of a linear relationship amongst voxels exhibiting progressive signal delays. In this work, we have expanded this model to account for non-linear onset behavior throughout the brain by characterizing signal ‘edges’ using a non-linear 3rd order spline fit (Bhogal, 2021). Moreover, we extended the carpet plot algorithm to map values back to the native functional space in order to generate spatial maps of blood arrival. Our reported gTTs were derived using the original code provided by Fitzgerald et al. (2021). Briefly, the transit time was defined by the difference in onset time between the voxel with the longest lag (top of the lag-sorted carpet plot) and the voxel with the shortest lag (bottom of the lag-sorted carpet plot).

Based on our experience, the transition from hypoxia to normoxia occurred more rapidly than from normoxia to hypoxia. Blood re-oxygenation can be affected the lung is faster than deoxygenation as a result of more favorable available range of pO_2 gradients. As a result, we chose to fit the onset edges around the two transitions to normoxia (see Fig. 1). Onset maps were calculated by averaging the voxel-wise onset values generated from both edges. We also averaged the two resulting transit time values for each subject.

The same hemodynamic lag and carpet plot analysis was performed on data derived using hypercapnic step + ramp stimuli obtained in one of the healthy controls and also a patient with unilateral carotid artery stenosis. For the hypercapnic cases, the $P_{ET}CO_2$ was used as the input for the analysis described above. Due to the nature of the hypercapnic stimulus (i.e. a block followed by a ramp), the return to baseline $P_{ET}CO_2$ was chosen for onset edge detection, since the progressive signal increase of the ramp stimulus did not provide sharp enough signal transitions.

2.5. Spatial normalization and statistical analysis

The mean BOLD image was spatially registered to the anatomical T1 scan using FSL’s (Jenkinson et al., 2012) FLIRT (Jenkinson and

Smith, 2001) function and resulting transformation matrices were inverted. The anatomical image was brain extracted (BET (Smith, 2002)) and then segmented (FAST (Zhang et al., 2001)) and the resulting tissue masks were transformed to BOLD space using the inverted transformation matrices; these masks were used in the analysis steps described in 2.1-2.2. The T1 image was then registered to the 2mm MNI atlas using linear (FLIRT) and non-linear (FNIRT (Jenkinson et al., 2012)) registration. Transformation matrices were then applied to the hemodynamic parameters to normalize the individual lag maps, hypoxic response, BOLD-CVR maps, and onset maps to MNI space. MNI-registered data was averaged and mean and standard deviation of regional hemodynamic values were calculated using a series of MNI regions of interest (ROI) masks. Where reported, statistical significance ($p < 0.01$) was investigated without the assumption of equal variance using a Welch’s *t*-test.

3. Results

3.1. Group comparison

All subjects were able to complete the hypoxic SHOCS protocol and reported no discomfort. The average respiration rates measured by the RespirAct system during the baseline period, versus the epoch between the moment our hypoxic target was reached until baseline $P_{ET}O_2$ was re-established after the second hypoxic block were 17.2 ± 4 and 17.3 ± 4.1 , respectively (paired *t*-test, not significantly different, $p = 0.79$). Individual subject $P_{ET}O_2$ traces aligned with the corresponding average GM SHOCS signal response data are provided in Fig. S2A/B. Based on the Severinghaus equation (Severinghaus, 1979) (see also the equations of Balaban et al. (2013)), the arterial saturation changed from approximately 98% to 75% between arterial partial of oxygen (PaO_2) of 95 mmHg to 40 mmHg (Fig. 1A). In general, the carpet plot analysis

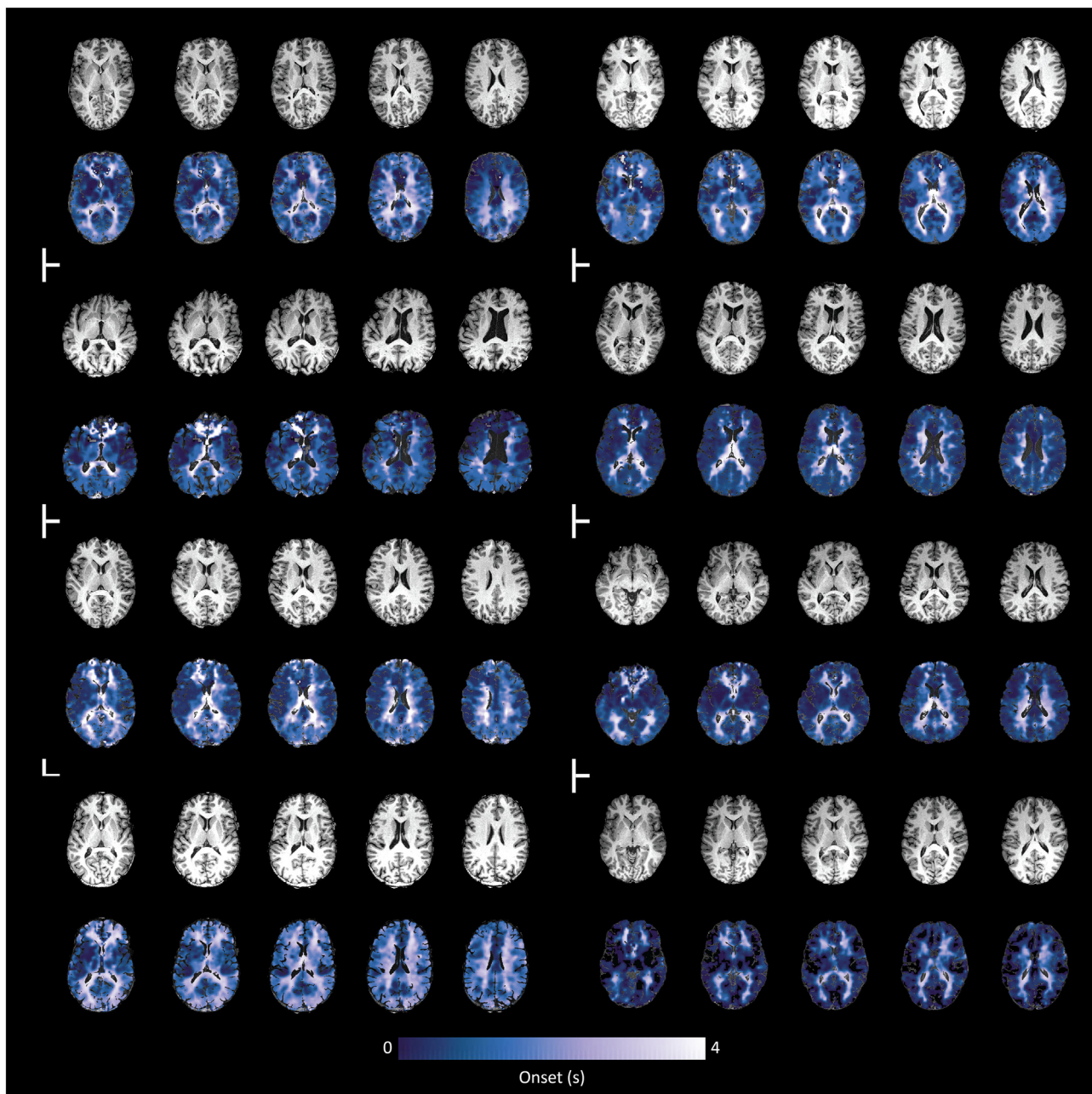


Fig. 2. Representative onset maps normalized to anatomical T1 image for 8 subjects: SHOCS onset times are scaled between 0 and 4 s. Onset maps represent arterial arrival time and show remarkable inter-subject stability within this range. Associated $P_{ET}O_2$ traces and aligned GM responses for all subjects are provided in Fig. S2A and carpet plots are provided in Fig. S3A.

based on the hypoxic challenge delivered consistent onset/blood arrival maps across all 12 healthy subjects with values ranging between 0 and 4 s (Fig. 2). Compared with the MNI-averaged hemodynamic lag maps, MNI-averaged onset maps demonstrated less spurious values; for example, in deeper WM where blood volume and the related BOLD contrast to noise ratio (CNR) can be low (see Fig. 3).

Mean and standard deviation lag, onset and hypoxic response values calculated in a series of MNI-ROIs are provided in Table 1. Consistent with known differences in cerebral blood volume (Leenders et al., 1990), the hypoxic signal response in cortical GM was approximately 1.7-fold higher than that measured in the deep WM (0.05 ± 0.02 versus $0.03 \pm 0.01\% \Delta BOLD / mmHg P_{ET}O_2$, respectively). Considering the assumption that the short hypoxic stimulus applied has limited effect on

vascular tone or tissue metabolism, this distribution suggests that the regional amplitude of the signal change may provide an indication of relative total blood volume (Fig. 3: right). When looking at regional onset times, the average onset of the occipital lobe was significantly longer than that of the frontal lobe (1.5 ± 0.4 versus 0.9 ± 0.4 s, $p < 0.001$), which is in line with expectations considering that the posterior circulation may be delayed due to the smaller diameter of vertebral artery and other anatomic variations. In the original work of Fitzgerald et al. (2021), the gTT as calculated using the carpet plot technique, is assumed to represent the propagation time of signal patterns throughout the majority of voxels in the brain. The gTT (as calculated by averaging the values from both edges in our data: see supplemental Fig. 2) was 4.5 ± 0.9 s across twelve subjects.

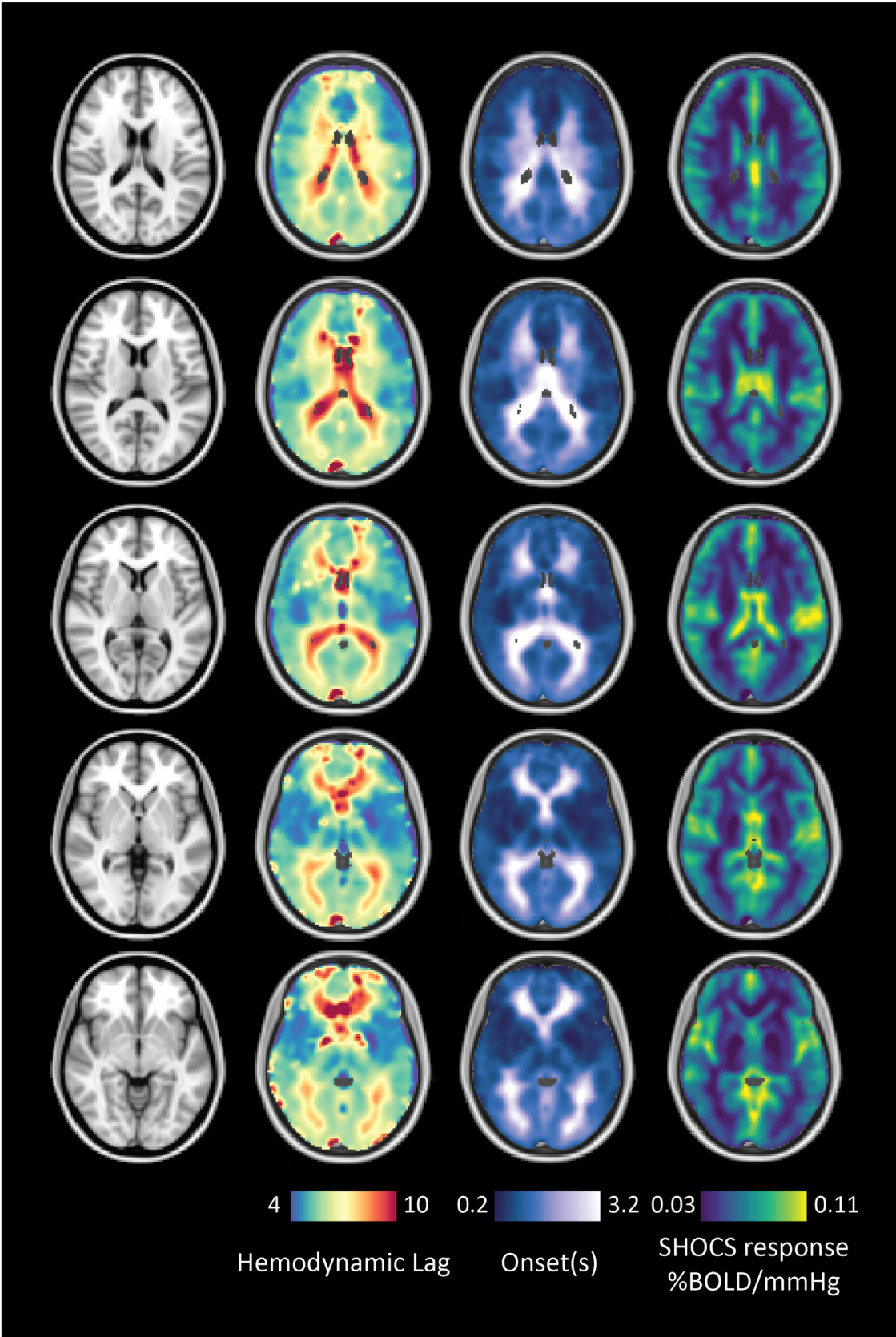


Fig. 3. *MNI averaged hemodynamic lag, onset and SHOCS response for 12 subjects:* regional average parameter responses are provided in [Table 1](#). Average maps have been smoothed using a 3D Gaussian kernel with 4mm FWHM.

Table 1

Mean and standard deviation calculated in MNI-averaged regions of interest (see Fig. 3). In the left column, MNI regions are sorted based on descending average lag values. On the right, MNI regions are sorted based on descending onset values. The SHOCS response is sorted in accordance with the onset times.

Region (Lag-sorted)	Lag	Region (Onset-sorted)	Onset	SHOCS Response
caudate	8.2 ± 1.5	caudate	2.0 ± 0.6	0.05 ± 0.01
deep white matter	7.8 ± 0.7	deep white matter	1.9 ± 0.6	0.03 ± 0.01
white matter	7.0 ± 1.3	thalamus	1.7 ± 0.9	0.07 ± 0.02
cerebellum	6.9 ± 1.1	white matter	1.6 ± 0.8	0.04 ± 0.02
frontal lobe	6.8 ± 2.0	cerebellum	1.5 ± 0.3	0.06 ± 0.02
occipital lobe	6.8 ± 1.0	occipital lobe	1.5 ± 0.5	0.05 ± 0.01
thalamus	6.8 ± 1.3	hippocampus	1.3 ± 0.4	0.06 ± 0.02
temporal	6.7 ± 1.9	parietal lobe	1.1 ± 0.6	0.05 ± 0.01
cortical grey matter	6.6 ± 1.5	temporal	1.1 ± 0.5	0.05 ± 0.02
parietal lobe	6.5 ± 0.9	cortical grey matter	1.1 ± 0.4	0.05 ± 0.02
hippocampus	6.4 ± 0.9	insula	0.9 ± 0.5	0.05 ± 0.02
putamen	5.8 ± 0.8	frontal lobe	0.9 ± 0.4	0.05 ± 0.02
insula	5.7 ± 0.8	putamen	0.9 ± 0.4	0.04 ± 0.01

3.2. Hypoxia versus hypercapnia

The average lag and onset values between GM and WM for the single subjects in which both protocols were performed were as follows: For hypercapnia, lag values were 15.8 ± 17.2 and 32.4 ± 23.4 s for GM and deep WM, respectively. Onset values were 4.0 ± 4.2 and 11.6 ± 9.0 s for GM and WM, respectively. For hypoxia, lag values were 5.9 ± 3.9 and 6.0 ± 2.7 s for GM and deep WM, respectively. Onset values were 1.3 ± 0.8 and 1.5 ± 1.0 s for GM and deep WM, respectively. Differences in spatial coverage and acquisition parameters between hypercapnic and hypoxic acquisitions limit in-depth comparison. However the tendency towards longer response times for hypercapnia was visibly obvious (see Figs. 4A, S3B).

3.3. Hypoxia versus hypercapnia in unilateral carotid artery occlusion

Consistent with the healthy subject example in Fig. 4, hemodynamic lag for both hypercapnic and hypoxic protocols showed consistent spatial distributions. With hypercapnia as the stimulus, hemodynamic lags were elevated in the healthy hemisphere, suggesting possible inter-hemispheric steal effects. In contrast, the contralateral hemisphere in the hypoxic case showed normal appearing hemodynamic lag (as did most of the GM tissue in the affected hemisphere); this translated to normal onset times (between 0 – 4 s) in the unaffected side but longer onset times in the affected hemisphere. The mean transit time across the brain was calculated at 5 s (Fig. S3), with highest onset values located in the affected hemisphere.

Response characteristics diverged when examining the CVR and hypoxic signal response. As previously determined, hypercapnic stimulus can evoke a vascular steal response, showing widespread re-distribution of blood flow and negative BOLD responses (Sobczyk et al., 2014). These pathological responses did manifest in the patient CO₂ example and compromised the utility of the carpet analysis. The hypoxic signal response remained consistent across hemispheres.

4. Discussion

In this work, ‘re-oxygenation’ challenges were applied in combination with dynamic BOLD imaging to provide a novel means through which to increase sensitivity weighting towards blood arrival and total blood volume, without the confounding effects related to dynamic vascular responses (Poubanc et al., 2015). Our main finding is that the onset values derived via our modified carpet plot analysis show remarkably consistent temporal distributions, which we consider to represent relative BAT. We report, for the first time, average regional hypoxic response values (expressed as %BOLD/mmHg P_{ET}CO₂) that are representative of relative total blood volume. Finally, comparison with BOLD-CVR

responses, SHOCS signals appear less confounded by dynamic response effects.

The signal onset times reported in our work support the notion that our SHOCS technique provides a possible additional means to investigate blood arrival and collateralization of blood flow. Similar to the DSC technique, preliminary work combining SHOCS have shown promise in delivering similar hemodynamic metrics as their more invasive counterpart. For instance, Vu et al., reported MTT values on the order of 8–9 s based on tracer kinetic modeling using a deoxygenated contrast bolus (Vu et al., 2021). Using similar methodology, Poubanc et al., reported MTT more in line with physiological ranges expected based on DSC work, at of 3.9 ± 0.6 s and 5.5 ± 0.6 for GM and WM, respectively (Ibaraki et al., 2006). Using a hyperoxic bolus, Macdonald et al. were able to derive MTTs of 2.94 ± 0.52 and 3.73 ± 0.60 s for GM and WM despite their insensitivity to arterial contributions. The differences in transit time measured using the hypoxic stimuli may be attributed to differences in the way the hypoxic bolus was administered. Specifically, Poubanc et al. were able to precisely target arterial O₂ pressure using a computer controlled system.

Whereas DSC (and SHOCS) is sensitive to both inflow and outflow of the contrast bolus, ASL-based studies have reported temporal metrics focused mainly on arterial transit times or bolus arrival times. In our method, onset times are reported relative to an internal reference consisting of the first voxels showing the earliest signal onset (i.e. the lowest lines of the carpet plot), whereas AAT and BAT are calculated relative to the time of the labeling pulse. Using multi-PLD pseudo-continuous ASL, Tsujikawa et al., reported increased AAT in affected brain hemispheres of patients with chronic occlusive disease (15 patients: 1.51 ± 0.41 s versus and 1.12 ± 0.30 contra-laterally) (Tsujikawa et al., 2016). Using pulsed ASL, MacIntosh et al., observed significantly longer arrival times in the occipital versus temporal lobes at 0.61 ± 0.10 and 0.94 ± 0.11 s, respectively. Interestingly, similar regional differences are observed in our work (see Table 1), along with a clear increases in the affected hemisphere of the patient example (Fig. 5). Overall, the SHOCS onset times fall between those reported using ASL (arterial only) and DSC (total vasculature). A strength of SHOCS over ASL is its sensitivity to WM responses.

Dynamic BOLD weighted functional MR imaging (fMRI) performed in either the resting-state (rsfMRI) or throughout hypercapnic gas challenges have also been proposed as methods through which to derive temporal perfusion information. In the case of CO₂ inhalation, this is done through the assessment of hemodynamic lag (Aso et al., 2017; Tong and Bd, 2012, 2014), however the hypercapnia-induced response can be slow and depends on the remaining vasodilatory reserve capacity, CO₂ sensitivity (Bhogal et al., 2014; Thomas et al., 2013) and vascular response speed (Poubanc et al., 2015). This can drive longer hemodynamic lag in WM regions (Bhogal et al., 2015;

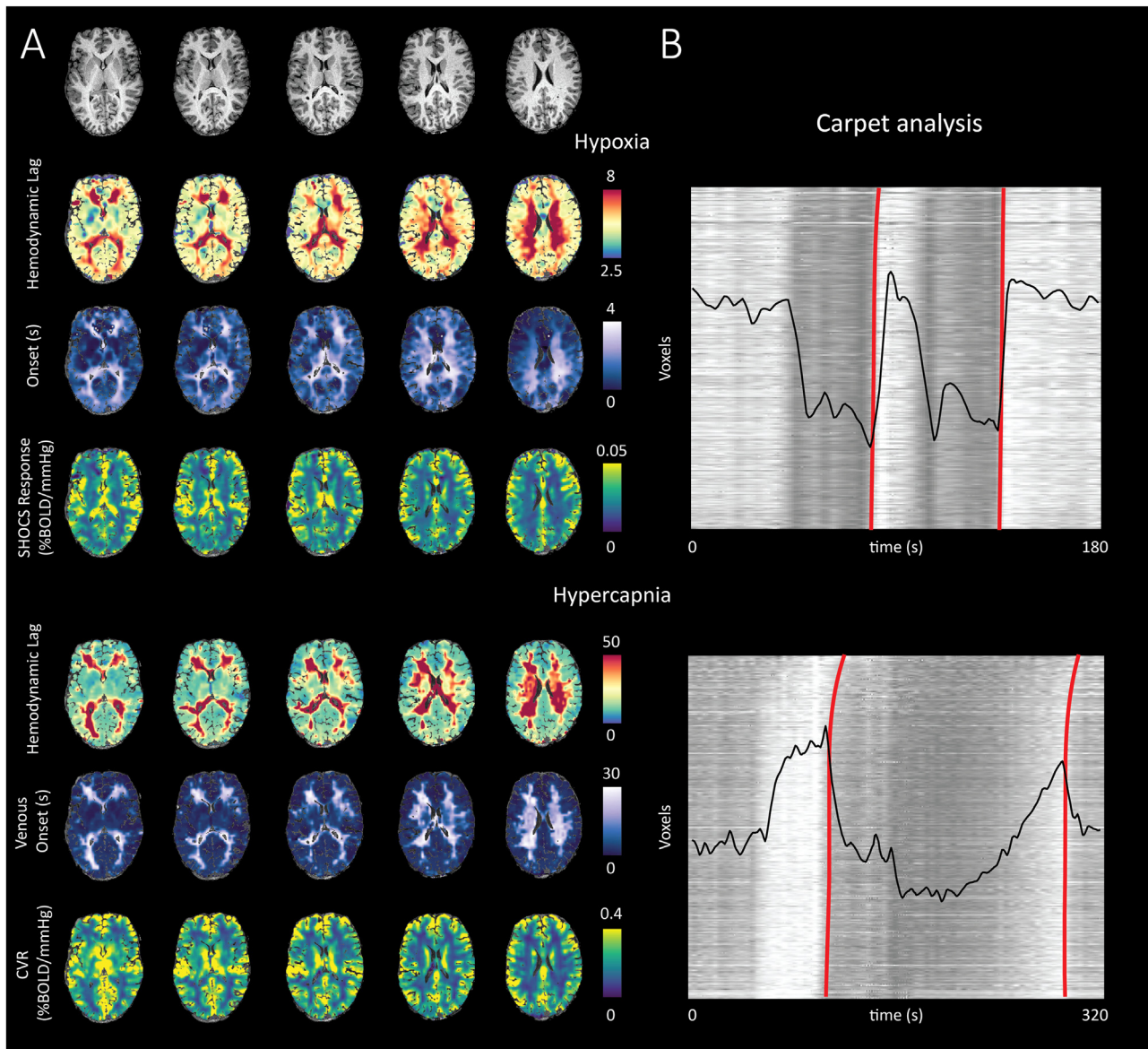


Fig. 4. Comparison of hemodynamic parameters generated using hypercapnic versus SHOCS in a single subject (A): in general, lag and onset values were considerably longer when based on the hypercapnic stimulus. This is likely due to insensitivity towards arterial signals and true response onset times. The CVR based lag analysis is more highly influenced by vascular resistance mediated flow redistribution, differential sensitivity to CO_2 (Thomas et al. (2013)) and vascular response rate (Poulblanc et al., 2015), as well as venous draining topology (Bhogal, 2021); (B) carpet plot results fitting the rising edge of the return to normoxia (top) during hypoxic experiments and the falling edge to baseline for hypercapnic experiments (bottom); the descending edge was chosen due to the limited onset contrast generated during the progressive CO_2 increase. Black traces represent the whole brain BOLD signal responses.

Thomas et al., 2013; Champagne and Bhogal, 2021), which is weighted by the response TTP, or blood redistribution effects and the vascular steal phenomenon (Sobczyk et al., 2014) shown in Fig. 5. Moreover, signals are subject to additional dispersion effects related to cerebral draining architecture which can influence local deoxy-hemoglobin concentrations (Bhogal, 2021) and obscure true blood arrival or transit times. Interestingly, systemic low frequency (sLFO) based perfusion information derived from rsfMRI is often thought of as physiological ‘noise’ which should be removed in order to better capture signal fluctuations originating from neuronal activation (Aso et al., 2019; Erdoğan et al., 2016; Tong et al., 2011). Cerebral circulation times derived from sLFO analysis have yielded whole brain transit times of approximately 5–7 s when comparing signals from large cerebral input arteries and output veins (Tong et al., 2019; Yao et al., 2019). Additionally, whole-brain correla-

tion based procedures carried out using 487 subjects from the Human Connectome Project Data have yielded lag times throughout the brain ranging up to 6 s (Tong et al., 2019) with spatial distributions very similar to those shown in Fig. 3. This raises the point that a hindrance to robust sLFO-based lag estimation arises from the relatively low CNR of blood-borne signals, which necessitate the averaging of many subjects. While this may limit the sensitivity of rsfMRI-based techniques to deliver robust single-subject temporal information (Nishida et al., 2019), sLFO-based perfusion information has proven sensitive enough to detect physiological changes associated with ageing and traumatic injury on a group-level (Aso et al., 2020). However, it should be noted that both sLFO and hypercapnia-based temporal mapping techniques show poor sensitivity when applied to the entirety of the arterial vascular network, and this should be taken into consideration when judging the accuracy

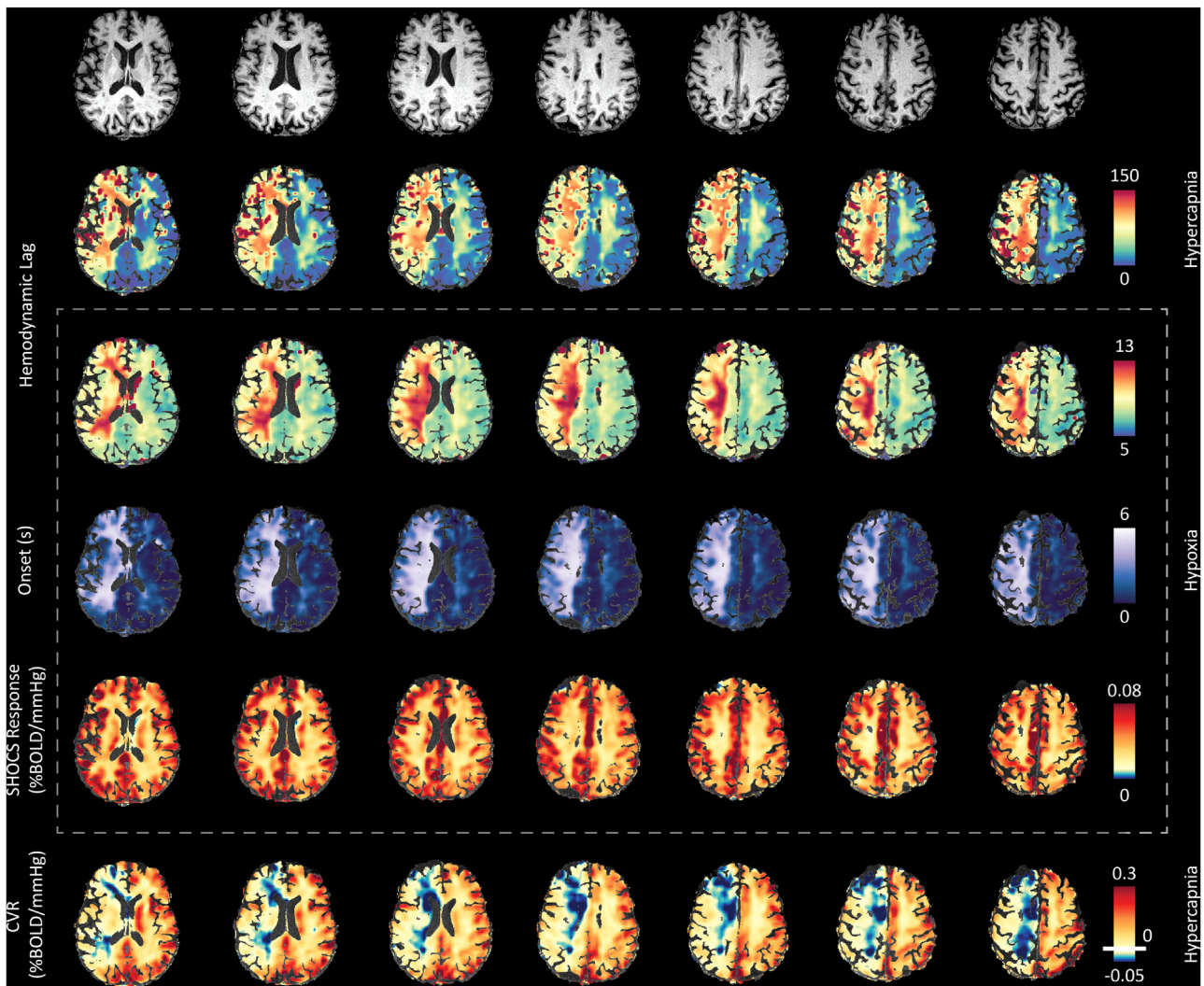


Fig. 5. Comparison of hemodynamic parameters generated using hypercapnic SHOCS in a patient with unilateral carotid artery occlusion. Similar to the healthy control case in Fig. 4, hemodynamic lag distribution was consistent between hypercapnic and SHOCS paradigms (rows 2 and 3). However, CO₂-mediated lag values were considerably longer and indicated altered flow dynamics in contralateral WM. Unilateral disease can result in bilateral impairment via redistribution effects through collateral networks (Deckers et al., 2021; Sam et al., 2015). Onset times derived using the hypoxic protocol remained consistent with controls in the unaffected hemisphere (0 to 4 s; Fig. 2) while onset time increased in the affected hemisphere (up to 5 s) consistent with presumably elongated transit times associated with collateralization or slower blood flow velocities (carpet plot is provided in Fig. S2B). SHOCS response maps (row 5) showed symmetric responses indicating robust blood arrival, while CVR maps (row 6) indicated negative responses related to vascular steal and exhausted vascular reserve capacity in the affected hemisphere. Since these effects generate variable signal responses, impaired reactivity can render the carpet plot analysis unfeasible when using hypercapnia (see Fig. S2B). *NOTE, CVR color-scale has been adapted compared to Fig. 3 and 4 in order to highlight negative CVR responses (vascular steal effect) in this patient example.

of blood arrival time, transit time or collateral blood flow; particularly when comparing to techniques such as ASL, DCE and now potentially SHOCS.

A further proposition of interest is that SHOCS can be used to measure total blood volume. This is because the SHOCS signal arises from both arterial and venous compartments combined. Of note however, is that at 3T, the gradient echo BOLD signal is comprised of intravascular and extravascular signal contributions that scale differently with changes in arterial and venous hemoglobin saturation (S_{aO_2} and S_{vO_2}) (Kim and Ogawa, 2012). These differential contributions obscure the ability to accurately estimate absolute CBV. Another important distinction is that the SHOCS contrast depends on local hematocrit, which may be variable throughout the brain irrespective of the local blood volume due to effects such as plasma skimming (Rosenblum, 1972). This is in contrast to DSC-CBV measurements using gadolinium injection, where the susceptibility contrast agent flows freely within the blood plasma. Nevertheless, vascular volume fraction as measured using ¹⁵O PET has

been reported as approximately 1.93 fold higher in GM ($5.2 \pm 1.4\%$) versus WM ($2.7 \pm 0.6\%$) which is similar to the 1.7 fold increase in SHOCS signal response between GM and deep WM (Leenders et al., 1990). A combination of advanced signal modeling and acquisition at higher magnetic field strength (7T+), where intravascular signal can be considered negligible (Uludağ et al., 2009), may provide a means for more accurate SHOCS-CBV estimation.

A potential confound to this application of SHOCS is that prolonged hypoxia is known to increase CBF (Cohen et al., 1967; Jensen et al., 2018). However, the response dynamics seem more sluggish when compared to commonly used vasodilators such as inhaled carbon dioxide. The work of Harris et al. (2013), reported a 15.4% increase in hypoxia-modulated CBF, with an Δ CBF onset delay of 185 s and a ΔR_2^* onset delay of 24 s when transitioning from normoxia to hypoxia and a non-significant delay when returning to baseline arterial oxygen partial pressure. Using transcranial Doppler measurements at the middle cerebral artery to observe the temporal dynamic of CBF responses to hypoxia,

Poulin et al. (1996) reported asymmetric time constants while decreasing arterial O_2 saturation (80 s) versus the return to normoxia (29 s). In line with the aforementioned results, we also observed more rapid BOLD signal transitions when inducing normoxia as opposed to hypoxia (Fig. S2). This asymmetric response may be explained by the presence of more plasma-dissolved O_2 during the baseline state that was available to bind to hemoglobin during the initial transition to hypoxia. The temporal asymmetry may also reflect the RespirAct system, which requires multiple breathing cycles to establish hypoxia, but is able to transition back to normoxia within one breath. This is related to the large gradient between lung pO_2 at approximately 100 mmHg, and the maximum atmospheric pO_2 of 760 mmHg at sea level, which sets up a the possibility to establish strong gradients for re-oxygenation. Our BOLD signal response features confirmed a negligible CBF effect due to the absence of a 'return to baseline' response time constant as reported by Poulin et al. (1996), and guided our decision to quantify onset using the rising, rather than falling response edges during the carpet plot analysis.

5. Considerations

The main consideration of our work relates to the use of hemodynamic lag values to sort carpet plot voxels. This approach means that the onset times can be influenced by the accuracy of the lag calculation, potentially leading to errors in cases where voxels are temporally mislabeled and therefore improperly ordered with respect to the edge calculation. Our preliminary comparison suggests that this approach is more reliable for hypoxia compared to hypercapnia due to the obvious sharper transitions and lack of dynamic response effects (see Fig. S3). Alternative ways of sorting (particularly for CO_2 -mediated changes) could be based on signal dispersion (defined as 'Tau' in the work of Poubanc et al. (2015)). Using this approach, onset times could then also be fit explicitly using a gamma variate function (Bhogal, 2021). Nevertheless, regions with limited (e.g. deep WM) or impaired CVR will not provide any meaningful information with respect to arrival time when using a CO_2 stimulus. In pathological cases exhibiting vascular steal phenomenon, the inverse polarity of the signal response in steal versus healthy regions will hinder the edge detection due to a mixing of rising and falling responses (see Fig. S3B).

In the original work of Fitzgerald et al., transit times generated using BOLD represented venous transit time (assumed to be whole brain). Our updated method using SHOCS, is sensitive to arterial onset (i.e. entry of the bolus into arterial voxels) as we cannot distinguish between arterial and venous signals. We suggest the deoxygenated bolus induces a bi-phasic response: initially as de-oxygenated (SAO_2 approx. 75%) blood enters arteries, followed by a second peak as the hypoxic bolus enters the venous system. Based on MRI measurements of resting venous saturation (SV_{O_2}) using T2-Relaxation-Under-Spin-Tagging (TRUST) (Lu and Ge, 2008) MRI, Deckers et al. (2022) reported SV_{O_2} on the order of 60-70% while breathing room air. Under the assumption that hypoxic breathing is iso-metabolic, SV_{O_2} under hypoxia could be expected to drop to as little as 35-45%. This could manifest in a significant BOLD signal differences emanating from veins versus arteries. Exploring this hypothesis would require a considerably higher sampling rate and higher spatial resolution than what was used in the current study with an additional SV_{O_2} measurement to facilitate more in-depth physiological modelling. To investigate this, future experimental designed might include the use of ultra-high field MRI in combination with surface receive coils (Schellekens et al., 2021) or fast line-scanning approaches (Raimondo et al., 2021). Of further interest could be generation of hypoxic arrival time maps with perfusion metrics derived from the 'gold-standard' DSC method. Additionally, a systematic comparison between temporal characteristics derived via hypercapnic versus hypoxic (and perhaps hyperoxic) experiments is warranted to confirm our interpretations that were made based on data presented in Figs. 4 and 5. From a clinical perspective, the combination of our modified carpet plot analysis with SHOCS can provide insight into the status

of collateral flow networks. As shown in our patient example, SHOCS onset times reflect normal baseline perfusion even in a patient prone to development of vascular steal with hypercapnia. We believe the addition of SHOCS to elucidate flow characteristics at rest may help to further stratify the severity of vascular impairment in patients with abnormal CVR. This warrants exploring the addition of our method in the investigation of patients with a variety of cerebrovascular pathology.

6. Conclusion

Our SHOCS method can be used to provide a measure of arterial blood arrival time. In cases with exhausted reserve capacity or confounding flow effects such as vascular steal, SHOCS can potentially assess the extent of collateral flow pathways providing a valuable complement to clinical CVR measures.

Data and code availability

The analysis tools used to generate the results presented in this manuscript are freely available via the open-source seeVR toolbox (<https://github.com/abhogal-lab/seeVR>). MRI and physiological data can be made available based on the submission of a formal project outline. Anonymized data will be shared by request from any qualified investigator for purposes such as replicating procedures and results presented in the article, provided that data transfer is in agreement with the University Health Network and Health Canada legislation on the general data protection regulation

Funding

This work was supported by a Dutch research council talent grant awarded to Alex A. Bhogal (NWO VENI: The ischemic fingerprint, [VI.VENI.194.056]).

Declaration of Competing Interest

JAF, DJM contributed to the development of the automated end-tidal targeting device, RespirAct™ (Thornhill Research Inc., TRI) used in this study and have equity in the company. RespirAct™ is a non-commercial device built by TMI to enable measurement of CVR in scientific studies. OS and JD receive salary support from TRI. TRI provided no other support for the study. All other authors have no disclosures to report.

Credit authorship contribution statement

Alex A. Bhogal: Conceptualization, Formal analysis, Methodology, Resources, Software, Visualization, Writing – original draft, Writing – review & editing, Funding acquisition. **Ece Su Sayin:** Conceptualization, Data curation, Investigation, Methodology. **Julien Poubanc:** Conceptualization, Data curation, Investigation, Methodology. **James Duffin:** Conceptualization, Methodology, Supervision, Writing – review & editing. **Joseph A. Fisher:** Conceptualization, Methodology, Supervision, Writing – review & editing. **Olivia Sobczyk:** Conceptualization, Methodology, Supervision, Data curation, Project administration. **David J. Mikulis:** Conceptualization, Methodology, Supervision, Data curation, Resources, Project administration, Writing – review & editing, Funding acquisition.

Data availability

Data will be made available on request.

Supplementary materials

Supplementary material associated with this article can be found, in the online version, at doi:[10.1016/j.neuroimage.2022.119523](https://doi.org/10.1016/j.neuroimage.2022.119523).

References

- Aso, T., Jiang, G., Fukuyama, H., 2017. A resilient, non-neuronal source of the spatiotemporal lag structure detected by BOLD signal-based blood flow tracking. *Front. Neurosci.* 11.
- Aso, T., Sugihara, G., Murai, T., et al., 2020. A venous mechanism of ventriculomegaly shared between traumatic brain injury and normal ageing. *Brain A J. Neurol.* 143 (6), 1843–1856.
- Aso, T., Urayama, S., Fukuyama, H., Murai, T., 2019. Axial variation of deoxyhemoglobin density as a source of the low-frequency time lag structure in blood oxygenation level-dependent signals. *PLoS One* 14 (9), e0222787.
- Balaban, D.Y., Duffin, J., Preiss, D., et al., 2013. The *in-vivo* oxyhaemoglobin dissociation curve at sea level and high altitude. *Respir. Physiol. Neurobiol.* 186 (1), 45–52.
- Bhogal, A.A., Philippens, M.E., Siero, J.C., et al., 2015. Examining the regional and cerebral depth-dependent BOLD cerebrovascular reactivity response at 7T. *Neuroimage* 114, 239–248.
- Bhogal, A.A., Siero, J.C., Fisher, J.A., et al., 2014. Investigating the non-linearity of the BOLD cerebrovascular reactivity response to targeted hypo/hypercapnia at 7T. *Neuroimage* 98, 296–305.
- Bhogal, A.A., 2021. Medullary vein architecture modulates the white matter BOLD cerebrovascular reactivity signal response to CO₂: Observations from high-resolution T2* weighted imaging at 7T. *Neuroimage* 245, 118771.
- Bhogal, A.A., 2021. seeVR: a Toolbox for Analyzing Cerebrovascular Reactivity Data, v1.01. Zenodo.
- Buxton, R.B., Frank, L.R., Wong, E.C., Siewert, B., Warach, S., Edelman, R.R., 1998. A general kinetic model for quantitative perfusion imaging with arterial spin labeling. *Magn. Reson. Med.* 40 (3), 383–396.
- Champagne, A.A., Bhogal, A.A., 2021. Insights into cerebral tissue-specific response to respiratory challenges at 7T: evidence for combined blood flow and CO₂-mediated effects. *Front. Physiol.* 12, 601369.
- Cohen, P.J., Alexander, S.C., Smith, T.C., Reivich, M., Wollman, H., 1967. Effects of hypoxia and normocarbina on cerebral blood flow and metabolism in conscious man. *J. Appl. Physiol.* 23 (2), 183–189.
- Deckers, P.T., Bhogal, A.A., Dijkstra, M.B., et al., 2022. Hemodynamic and metabolic changes during hypercapnia with normoxia and hyperoxia using pCASL and TRUST MRI in healthy adults. *J. Cereb. Blood Flow Metab.* 0 (0), 0271678X211064572.
- Deckers, P.T., van Hoek, W., Kronenburg, A., et al., 2021. Contralateral improvement of cerebrovascular reactivity and TIA frequency after unilateral revascularization surgery in moyamoya vasculopathy. *NeuroImage Clin.* 30, 102684.
- Donahue, M.J., Faraco, C.C., Strother, M.K., et al., 2014. Bolus arrival time and cerebral blood flow responses to hypercarbia. *J. Cereb. Blood Flow Metab.* 34 (7), 1243–1252. *Off. J. Int. Soc. Cereb. Blood Flow Metab.*
- Donahue, M.J., Strother, M.K., Lindsey, K.P., Hocke, L.M., Tong, Y., Frederick, B.D., 2016. Time delay processing of hypercapnic fMRI allows quantitative parameterization of cerebrovascular reactivity and blood flow delays. *J. Cereb. Blood Flow Metab.* 36 (10), 1767–1779 official journal of the International Society of Cerebral Blood Flow and Metabolism.
- Duffin, J., Sobczyk, O., Crawley, A., et al., 2017. The role of vascular resistance in BOLD responses to progressive hypercapnia. *Hum. Brain Mapp.* 38 (11), 5590–5602.
- Erdogan, S.B., Tong, Y., Hocke, L.M., Lindsey, K.P., deB Frederick, B., 2016. Correcting for blood arrival time in global mean regression enhances functional connectivity analysis of resting state fMRI-BOLD signals. *Front. Hum. Neurosci.* 10.
- Fitzgerald, B., Yao, J.F., Talavage, T.M., Hocke, L.M., Frederick, B.D., Tong, Y., 2021. Using carpet plots to analyze transit times of low frequency oscillations in resting state fMRI. *Sci. Rep.* 11 (1), 7011.
- Frederick, B., Nickerson, L.D., Tong, Y., 2012. Physiological denoising of BOLD fMRI data using Regressor Interpolation at Progressive Time Delays (RIPTiDe) processing of concurrent fMRI and near-infrared spectroscopy (NIRS). *Neuroimage* 60 (3), 1913–1923.
- Harris, A.D., Murphy, K., Diaz, C.M., et al., 2013. Cerebral blood flow response to acute hypoxic hypoxia. *NMR Biomed.* 26 (12), 1844–1852.
- Hartkamp, N.S., Bokkers, R.P., van der Worp, H.B., van Osch, M.J., Kappelle, L.J., Hendrikse, J., 2011. Distribution of cerebral blood flow in the caudate nucleus, lentiform nucleus and thalamus in patients with carotid artery stenosis. *Eur. Radiol.* 21 (4), 875–881.
- Ibaraki, M., Ito, H., Shimosegawa, E., et al., 2006. Cerebral vascular mean transit time in healthy humans: a comparative study with PET and dynamic susceptibility contrast-enhanced MRI. *J. Cereb. Blood Flow Metab.* 27 (2), 404–413.
- Jenkinson, M., Beckmann, C.F., Behrens, T.E., Woolrich, M.W., Smith, S.M., 2012. FSL. *Neuroimage* 62 (2), 782–790.
- Jenkinson, M., Smith, S., 2001. A global optimisation method for robust affine registration of brain images. *Med. Image Anal.* 5 (2), 143–156.
- Jensen, M.L.F., Vestergaard, M.B., Tønnesen, P., Larsson, H.B.W., Jennum, P.J., 2018. Cerebral blood flow, oxygen metabolism, and lactate during hypoxia in patients with obstructive sleep apnea. *Sleep* 41 (3).
- Kim, S.G., Ogawa, S., 2012. Biophysical and physiological origins of blood oxygenation level-dependent fMRI signals. *J. Cereb. Blood Flow Metab.* 32 (7), 1188–1206 official journal of the International Society of Cerebral Blood Flow and Metabolism.
- Leenders, K.L., Perani, D., Lammertsma, A.A., et al., 1990. Cerebral blood flow, blood volume and oxygen utilization. Normal values and effect of age. *Brain* 113 (Pt 1), 27–47.
- Lou, X., Yu, S., Scalzo, F., et al., 2017. Multi-delay ASL can identify leptomeningeal collateral perfusion in endovascular therapy of ischemic stroke. *Oncotarget* 8 (2), 2437–2443.
- Lu, H., Ge, Y., 2008. Quantitative evaluation of oxygenation in venous vessels using T2-relaxation-under-spin-tagging MRI. *Magn. Reson. Med.* 60 (2), 357–363.
- McVerry, F., Liebeskind, D.S., Muir, K.W., 2012. Systematic review of methods for assessing leptomeningeal collateral flow. *Am. J. Neuroradiol.* 33 (3), 576–582.
- Nishida, S., Aso, T., Takaya, S., et al., 2019. Resting-state functional magnetic resonance imaging identifies cerebrovascular reactivity impairment in patients with arterial occlusive diseases: a pilot study. *Neurosurgery* 85 (5), 680–688.
- Okell, T.W., Harston, G.W.J., Chappell, M.A., Sheerin, F., Kennedy, J., Jezzard, P., 2019. Measurement of collateral perfusion in acute stroke: a vessel-encoded arterial spin labeling study. *Sci. Rep.* 9 (1), 8181.
- Paling, D., Thade Petersen, E., Tozer, D.J., et al., 2014. Cerebral arterial bolus arrival time is prolonged in multiple sclerosis and associated with disability. *J. Cereb. Blood Flow Metab.* 34 (1), 34–42 official journal of the International Society of Cerebral Blood Flow and Metabolism.
- Poulblanc, J., Crawley, A.P., Sobczyk, O., et al., 2015. Measuring cerebrovascular reactivity: the dynamic response to a step hypercapnic stimulus. *J. Cereb. Blood Flow Metab.* 35 (11), 1746–1756 official journal of the International Society of Cerebral Blood Flow and Metabolism.
- Poulblanc, J., Sobczyk, O., Shafi, R., et al., 2021. Perfusion MRI using endogenous deoxyhemoglobin as a contrast agent: preliminary data. *Magn. Reson. Med.* 86 (6), 3012–3021.
- Poulin, M.J., Liang, P.J., Robbins, P.A., 1996. Dynamics of the cerebral blood flow response to step changes in end-tidal PCO₂ and PO₂ in humans. *J. Appl. Physiol.* 81 (3), 1084–1095.
- Raimondo, L., Knapen, T., ÁF, O., et al., 2021. A line through the brain: implementation of human line-scanning at 7T for ultra-high spatiotemporal resolution fMRI. *J. Cereb. Blood Flow Metab.* 41 (11), 2831–2843.
- Rosenblum, W.I., 1972. Can plasma skimming of inconstancy of regional hematocrit introduce serious errors in regional cerebral blood flow measurements or their interpretation? *Stroke* 3 (3), 248–254.
- Sam, K., Poulblanc, J., Sobczyk, O., et al., 2015. Assessing the effect of unilateral cerebral revascularisation on the vascular reactivity of the non-intervened hemisphere: a retrospective observational study. *BMJ Open* 5 (2), e006014.
- Schellekens W., Bhogal A.A., Roefs E.C.A., Báez-Yáñez M.G., Siero J.C.W., Petridou N., The many layers of BOLD. On the contribution of different vascular compartments to laminar fMRI. *bioRxiv*. 2021:2021.2010.2021.465359.
- Sebök, M., Esposito, G., Niftrik, C., et al., 2022. Flow augmentation STA-MCA bypass evaluation for patients with acute stroke and unilateral large vessel occlusion: a proposal for an urgent bypass flowchart. *J. Neurosurg.* 1–9.
- Sebök, M., Niftrik, C., Lohaus, N., et al., 2021. Leptomeningeal collateral activation indicates severely impaired cerebrovascular reserve capacity in patients with symptomatic unilateral carotid artery occlusion. *J. Cereb. Blood Flow Metab.* 41 (11), 3039–3051 official journal of the International Society of Cerebral Blood Flow and Metabolism.
- Seiler, A., Brandhofe, A., Gracien, R.M., et al., 2021. DSC perfusion-based collateral imaging and quantitative T2 mapping to assess regional recruitment of leptomeningeal collaterals and microstructural cortical tissue damage in unilateral steno-occlusive vasculopathy. *J. Cereb. Blood Flow Metab.* 41 (1), 67–81 official journal of the International Society of Cerebral Blood Flow and Metabolism.
- Severinghaus, J.W., 1979. Simple, accurate equations for human blood O₂ dissociation computations. *J. Appl. Physiol.* 46 (3), 599–602.
- Smith, S.M., 2002. Fast robust automated brain extraction. *Hum. Brain Mapp.* 17 (3), 143–155.
- Sobczyk, O., Battisti-Charbonney, A., Fierstra, J., et al., 2014. A conceptual model for CO₂-induced redistribution of cerebral blood flow with experimental confirmation using BOLD MRI. *Neuroimage* 92, 56–68.
- Sobczyk, O., Sam, K., Mandell, D.M., et al., 2020. Cerebrovascular reactivity assays collateral function in carotid stenosis. *Front. Physiol.* 11, 1031.
- Thomas, B.P., Liu, P., Park, D.C., van Osch, M.J.P., Lu, H., 2013. Cerebrovascular reactivity in the brain white matter: magnitude, temporal characteristics, and age effects. *J. Cereb. Blood Flow Metab.* 34 (2), 242–247.
- Tong, Y., Bd, F., 2012. Concurrent fNIRS and fMRI processing allows independent visualization of the propagation of pressure waves and bulk blood flow in the cerebral vasculature. *Neuroimage* 61 (4), 1419–1427.
- Tong, Y., Bd, F., 2014. Tracking cerebral blood flow in BOLD fMRI using recursively generated regressors. *Hum. Brain Mapp.* 35 (11), 5471–5485.
- Tong, Y., Hocke, L.M., Frederick, B.B., 2019. Low frequency systemic hemodynamic “noise” in resting state BOLD fMRI: characteristics, causes, implications, mitigation strategies, and applications. *Front. Neurosci.* 13, 787.
- Tong, Y., Lindsey, K.P., de, BFB., 2011. Partitioning of physiological noise signals in the brain with concurrent near-infrared spectroscopy and fMRI. *J. Cereb. Blood Flow Metab.* 31 (12), 2352–2362 official journal of the International Society of Cerebral Blood Flow and Metabolism.
- Tong, Y., Yao, J.F., Chen, J.J., Frederick, B.D., 2019. The resting-state fMRI arterial signal predicts differential blood transit time through the brain. *J. Cereb. Blood Flow Metab.* 39 (6), 1148–1160 official journal of the International Society of Cerebral Blood Flow and Metabolism.
- Tsujikawa, T., Kimura, H., Matsuda, T., et al., 2016. Arterial transit time mapping obtained by pulsed continuous 3D ASL imaging with multiple post-label delay acquisitions: comparative study with PET-CBF in patients with chronic occlusive cerebrovascular disease. *PLoS One* 11 (6), e0156005–e0156005.
- Uludağ, K., Müller-Bierl, B., Uğurbil, K., 2009. An integrative model for neuronal activity-induced signal changes for gradient and spin echo functional imaging. *Neuroimage* 48 (1), 150–165.
- van Osch, M.J., Teeuwisse, W.M., Chen, Z., Suzuki, Y., Helle, M., Schmid, S., 2018. Advances in arterial spin labelling MRI methods for measuring perfusion and collateral flow. *J. Cereb. Blood Flow Metab.* 38 (9), 1461–1480 official journal of the International Society of Cerebral Blood Flow and Metabolism.

- Vu, C., Chai, Y., Coloigner, J., et al., 2021. Quantitative perfusion mapping with induced transient hypoxia using BOLD MRI. *Magn. Reson. Med.* 85 (1), 168–181.
- Yao, J.F., Wang, J.H., Yang, H.S., et al., 2019. Cerebral circulation time derived from fMRI signals in large blood vessels. *J. Magn. Reson. Imaging JMRI* 50 (5), 1504–1513.
- Zaharchuk, G., 2020. Arterial transit awesomeness. *Radiology* 297 (3), 661–662.
- Zhang, Y., Brady, M., Smith, S., 2001. Segmentation of brain MR images through a hidden Markov random field model and the expectation-maximization algorithm. *IEEE Trans. Med. Imaging* 20 (1), 45–57.

Further reading

- Tong, Y., Lindsey, K.P., Hocke, L.M., Vitaliano, G., Mintzopoulos, D., Frederick, B.D., 2017. Perfusion information extracted from resting state functional magnetic resonance imaging. *J. Cereb. Blood Flow Metab.* 37 (2), 564–576 official journal of the International Society of Cerebral Blood Flow and Metabolism.